Progress In Electromagnetics Research, Vol. 143, 223–242, 2013

PARALLEL IMPLEMENTATION AND APPLICATION OF THE MRTD WITH AN EFFICIENT CFS-PML

Yawen Liu*, Yiwang Chen, and Pin Zhang

National Key Laboratory on Electromagnetic Environment and Electro-optical Engineering, PLA University of Science and Technology, Nanjing 210007, China

Abstract—In this paper, we describe two parallel MRTD algorithms. Both algorithms are proved to be feasible by comparing the result of the serial MRTD method, the efficiency of them are also compared in order to evaluate a better strategy. Moreover, a novel implementation of "complex frequency-shifted" perfect matched layer (CFS-PML) with auxiliary differential equation (ADE) is presented for the MRTD method. The implementation is easier to obtain and more memory saving when treating more generalized media, and numerical results demonstrate that the CFS-PML with ADE is more absorptive than the popularly used APML. Furthermore, using one of the parallel algorithms and the CFS-PML, the characteristic of the field cross-section distribution of the electromagnetic pulse (EMP) propagation in vaulted tunnel is studied.

1. INTRODUCTION

The Multi-Resolution Time-Domain (MRTD) technique was first published in 1996 by Krumpholz and Katehi [1, 2], and has been developed rapidly as an efficient numerical algorithm in the time-domain like the long established Finite Difference Time-Domain (FDTD) technique [3–17] and other time-domain methods [18–20]. As the dispersion of the MRTD scheme compared to the conventional FDTD scheme shows an excellent capability to approximate the exact solution with negligible error for sampling rates approaching the Nyquist limit, it becomes possible that larger targets can be simulated without sacrificing accuracy. However, owing to the limitation of the computer memory, the calculation can be only implemented in

Received 25 September 2013, Accepted 30 October 2013, Scheduled 1 November 2013

* Corresponding author: Yawen Liu (liuyawen1111@163.com).

a finite area. So, for the intensive computation and storage, there are some challenges for its practical implementation when dealing with the electrically large and complex electromagnetic structures. To overcome the computation power and storage requirement bottlenecks, this paper focuses on the parallel implementation of the S-MRTD based on Daubechies' compactly supported scaling functions with two vanishing moments [21, 22]. As the Message Passing Interface (MPI) [23] is becoming the new international standard for parallel programming, the MPI library is employed to exchange the electric and/or magnetic fields. We describe two parallel MRTD approaches, which of the efficiencies are compared in this paper. For the sake of simplicity and compactness, a parallel MRTD algorithm for the mode based on the one-dimension domain decomposition method is presented.

We also describe the CFS-PML [24] with auxiliary differential equation for the S-MRTD in detail. Numerical results show that the technique is more efficient at numerical reflection and memory saving than that of the widely used APML [25].

2. PARALLEL MRTD ALGORITHM

Just like the FDTD, MRTD is also nearly inherently parallel in nature since only local information is needed for updating the fields at each time increment. Parallel MRTD can be seen as a kind of algorithm that the whole computational domain is divided into several sub-domains and each node only handles for the corresponding sub-domains calculation. Therefore, the requirement of computational storage and CPU time is reduced several times, which implies that the parallel MRTD is faster than a serial counterpart almost by a factor n, where n is the number of processors.

2.1. MRTD Scheme

Maxwell's curl equations in the time domain

$$\left.\begin{aligned} \nabla \times \mathbf{E} &= -\mu \frac{\partial \mathbf{H}}{\partial t} - \sigma_m \mathbf{H} \\ \nabla \times \mathbf{H} &= \varepsilon \frac{\partial \mathbf{E}}{\partial t} + \sigma \mathbf{E} \end{aligned}\right\} \tag{1}$$

are discretized on the traditional Yee grid. As the theory in [21], the fields are expanded in Daubechies' compactly supported scaling functions ϕ [26], which approximately satisfy the shifted interpolation property [27]

$$\phi\left(k + M_1\right) = \delta_{k,0} \tag{2}$$

for k integer, where

$$M_1 = \int_{-\infty}^{+\infty} x\phi(x)dx \tag{3}$$

is the first-order moment of the scaling function and the Kronecker delta function. This property yields a simple algorithm for inhomogeneous problems through the local sampling of the field values regardless of the complexity of the inhomogeneity [21].

According to the wavelet-Galerkin scheme based on Daubechies' compactly supported wavelets, a system of updating equations similar to the S-MRTD [2] method can be obtained

$$E_{i+\frac{1}{2},j,k}^{\phi x,n+1} = CA_m E_{i+\frac{1}{2},j,k}^{\phi x,n} + CB_m \left[\frac{1}{\Delta y} \sum_l a(l) H_{i+\frac{1}{2},j+l+\frac{1}{2},k}^{\phi z,n+\frac{1}{2}} - \frac{1}{\Delta z} \sum_l a(l) H_{i+\frac{1}{2},j,k+l+\frac{1}{2}}^{\phi y,n+\frac{1}{2}} \right] \tag{4}$$

where

$$CA_m = \frac{2\varepsilon_m - \sigma_m \Delta t}{2\varepsilon_m + \sigma_m \Delta t} \tag{5}$$

$$CB_m = \frac{2\Delta t}{2\varepsilon_m + \sigma_m \Delta t} \tag{6}$$

the subscript $m = (i + 1/2,\ j,\ k)$. The coefficients $a(l)$ for $0 \le l \le 2$ have been tabulated in [28].

2.2. The First Domain Decomposition Method (DDM-I)

The DDM-I is shown in Fig. 1, this method uses an MPI function to send the $H_{x,y}(:, :, nk1-1)$, $H_{x,y}(:, :, nk1-2)$, $H_{x,y}(:, :, nk1-3)$ and $E_{x,y}(:, :, nk1-1)$, $E_{x,y}(:, :, nk1-2)$ from the processor N to $N+1$, and to calculate the $E_{x,y}(:, :, nk0)$, $E_{x,y}(:, :, nk0+1)$, $E_{x,y}(:, :, nk0+2)$ and $H_{x,y}(:, :, nk1-1)$, $H_{x,y}(:, :, nk1-2)$ in processor $N+1$. The MPI function is once again to send the $E_{x,y}(:, :, nk0)$, $E_{x,y}(:, :, nk0+1)$, $E_{x,y}(:, :, nk0+2)$ and $H_{x,y}(:, :, nk1-1)$, $H_{x,y}(:, :, nk1-2)$ from the processor $N+1$ to N.

2.3. The Second Domain Decomposition Method (DDM-II)

The DDM-II is shown in Fig. 2. In this approach, the MPI function is to send the $H_{x,y}(:, :, nk1-1)$, $H_{x,y}(:, :, nk1-2)$, $H_{x,y}(:, :, nk1-3)$, $H_{x,y}(:, :, nk1-4)$ and $H_{x,y}(:, :, nk1-5)$ from processor N to $N+1$, the $H_{x,y}$ in the processor N, received from the processor $N+1$, is then used

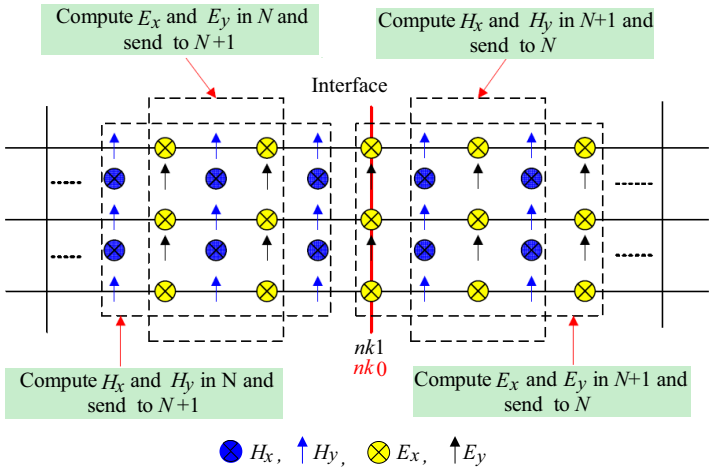

Figure 1. Two adjacent sub-domains.

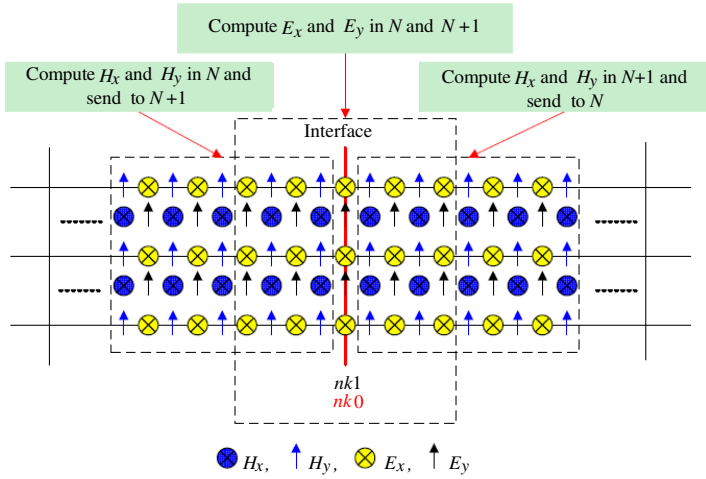

Figure 2. Sub-domains with three cells overlap.

to calculate the $E_{x,y}(:, :, nk0-2)$, $E_{x,y}(:, :, nk0-1)$, $E_{x,y}(:, :, nk0)$, $E_{x,y}(:, :, nk0+1)$ and $E_{x,y}(:, :, nk0+2)$ in the sub-domain N. The same procedure is then used in the processor $N+1$. Compared with the DDM-I, only the magnetic fields are exchanged in DDM-II, however, the $E_{x,y}$ above should be updated in both the processor N and $N+1$.

2.4. The Parallel MRTD Algorithms Using MPI

MPI is an international standard that supports message passing in a parallel processing system, and provides a standard environment for this purpose as well as a standard communication library. Based on MPI, a parallel computation can be composed of a number of processes, each works on some local data. The MPI standard defines interfaces to two languages, C and Fortran, and we use Fortran95 in programming in this paper.

According to the domain decomposition method mentioned above, the original problem is divided into several sub-domains in terms of the features of the problem. Each sub-domain is treated as a process, and MPI connects these processes together. Before a program is executed, the user sets the number of processors to be used.

A standard parallel MRTD algorithm consists of parallelism steps as follows:

a) MPI initialization.
b) Determination of the process number.
c) Reading and computation of simulation parameters.
d) Creation of the derived data types for communication purpose.
e) Start time iterations (time-stepping).
f) End.

3. APPLICATION OF CFS-PML TO MRTD METHOD

3.1. Formulation

In this section, the CFS-PML for MRTD based on Daubechies scaling functions is discussed. For the sake of generality example, a lossy medium is assumed here. In the PML layer, the formulation is posed in the stretched coordinate space [29]

$$j\omega\varepsilon E_x + \sigma E_x = \frac{1}{s_y}\frac{\partial}{\partial y}H_z - \frac{1}{s_z}\frac{\partial}{\partial z}H_y \tag{7}$$

where s_i are the stretched-coordinate metric, which are proposed to be

$$s_i = \kappa_i + \frac{\sigma_i}{\alpha_i + j\omega\varepsilon_0}, \quad i = x, y, z \tag{8}$$

and then we can get

$$\begin{cases} \dfrac{1}{s_i} = \dfrac{1}{\kappa_i} + \dfrac{\sigma_i'}{\alpha_i' + j\omega\varepsilon_i'} \\ \left(\sigma_i' = -\sigma_i, \quad \varepsilon_i' = \varepsilon_0\kappa_i^2, \quad \alpha_i' = \kappa_i^2\alpha_i + \kappa_i\sigma_i\right) \end{cases} \tag{9}$$

where σ_i, κ_i and α_i are nonnegative reals, and $\kappa_i \geq 1$. This choice for the variables was originally proposed by Kuzuoglu and Mittra [30].

Inserting (9) into (7), we obtain

$$\begin{aligned} j\omega\varepsilon E_x+\sigma E_x &= \frac{1}{\kappa_y}\frac{\partial}{\partial y}H_z-\frac{1}{\kappa_z}\frac{\partial}{\partial z}H_y+\frac{\sigma'_y}{\alpha'_y+j\omega\varepsilon'_y}\frac{\partial}{\partial y}H_z-\frac{\sigma'_z}{\alpha'_z+j\omega\varepsilon'_z}\frac{\partial}{\partial z}H_y \\ &= \frac{1}{\kappa_y}\frac{\partial}{\partial y}H_z-\frac{1}{\kappa_z}\frac{\partial}{\partial z}H_y+\varphi_{e_{xz}}-\varphi_{e_{xy}} \end{aligned} \tag{10}$$

where

$$\varphi_{e_{xy}} = \frac{\sigma'_y}{\alpha'_y+j\omega\varepsilon'_y}\frac{\partial}{\partial y}H_z \tag{11}$$

$$\varphi_{e_{xz}} = \frac{\sigma'_z}{\alpha'_z+j\omega\varepsilon'_z}\frac{\partial}{\partial z}H_y \tag{12}$$

Here we rewrite (11)–(12) as

$$j\omega\varepsilon'_y\varphi_{e_{xy}}+\alpha'_y\varphi_{e_{xy}} = \sigma'_y\frac{\partial}{\partial y}H_z \tag{13}$$

$$j\omega\varepsilon'_z\varphi_{e_{xz}}+\alpha'_z\varphi_{e_{xz}} = \sigma'_z\frac{\partial}{\partial z}H_y \tag{14}$$

then transform (10), (13) and (14) into time domain

$$\varepsilon\frac{\partial}{\partial t}E_x+\sigma E_x = \frac{1}{\kappa_y}\frac{\partial}{\partial y}H_z-\frac{1}{\kappa_z}\frac{\partial}{\partial z}H_y+\varphi_{e_{xz}}-\varphi_{e_{xy}} \tag{15}$$

$$\varepsilon'_y\frac{\partial\varphi_{e_{xy}}}{\partial t}+\alpha'_y\varphi_{e_{xy}} = \sigma'_y\frac{\partial}{\partial y}H_z \tag{16}$$

$$\varepsilon'_z\frac{\partial\varphi_{e_{xz}}}{\partial t}+\alpha'_z\varphi_{e_{xz}} = \sigma'_z\frac{\partial}{\partial z}H_y \tag{17}$$

Also for the sake of simplicity in the presentation and without loss of generality, the fields E_x, H_y and H_z the auxiliary variables $\varphi_{e_{xy}}$ and $\varphi_{e_{xz}}$ are expanded in terms of scaling functions only in space domain and pulse functions in time domain.

$$E_x(\vec{r},t) = \sum_{i,j,k,n=-\infty}^{+\infty} E^{\phi x,n}_{i+\frac{1}{2},j,k}h_n(t)\phi_i(x)\phi_j(y)\phi_k(z) \tag{18}$$

$$H_y(\vec{r},t) = \sum_{i,j,k,n=-\infty}^{+\infty} H^{\phi y,n+\frac{1}{2}}_{i+\frac{1}{2},j,k+\frac{1}{2}}h_{n+\frac{1}{2}}(t)\phi_{i+\frac{1}{2}}(x)\phi_j(y)\phi_{k+\frac{1}{2}}(z) \tag{19}$$

$$H_z(\vec{r},t)=\sum_{i,j,k,n=-\infty}^{+\infty} H^{\phi z,n+\frac{1}{2}}_{i+\frac{1}{2},j+\frac{1}{2},k} h_{n+\frac{1}{2}}(t)\phi_{i+\frac{1}{2}}(x)\phi_{j+\frac{1}{2}}(y)\phi_k(z) \quad (20)$$

$$\phi_{e_{xy}}(\vec{r},t)=\sum_{i,j,k,n=-\infty}^{+\infty} \phi^{\phi x,n}_{e_{xy},i+\frac{1}{2},j,k} h_n(t)\phi_{i+\frac{1}{2}}(x)\phi_j(y)\phi_k(z) \quad (21)$$

$$\phi_{e_{xz}}(\vec{r},t)=\sum_{i,j,k,n=-\infty}^{+\infty} \phi^{\phi x,n}_{e_{xz},i+\frac{1}{2},j,k} h_n(t)\phi_{i+\frac{1}{2}}(x)\phi_j(y)\phi_k(z) \quad (22)$$

where $E^{\phi x,n}_{i+\frac{1}{2},j,k}$, $H^{\phi y,n+\frac{1}{2}}_{i+\frac{1}{2},j,k+\frac{1}{2}}$, and $H^{\phi z,n+\frac{1}{2}}_{i+\frac{1}{2},j+\frac{1}{2},k}$, $\phi^{\phi x,n}_{e_{xy},i+\frac{1}{2},j,k}$ and $\phi^{\phi x,n+\frac{1}{2}}_{e_{xz},i,j,k+\frac{1}{2}}$ are the coefficients for the fields and the auxiliary variables expansions in terms of scaling functions which are equal to the corresponding fields and auxiliary variables. The indexes i, j, k, and n, are the discrete space and time indices related to the space and time coordinates via $x = i\Delta x$, $y = j\Delta y$, $z = k\Delta z$, and $t = n\Delta t$, where Δx, Δy, Δz, and Δt, represent the space and time discretization intervals in x-, y-, z- and t-direction. The function $h(t)$ is defined as Haar's scaling function, and ϕ is Daubechies' scaling function with two vanishing moments.

With the wavelet-Galerkin scheme based on Daubechies' compactly supported wavelets, a system of updating equations similar to the S-MRTD method can be obtained

$$E^{\phi x,n+1}_{i+\frac{1}{2},j,k} = CA_m E^{\phi x,n}_{i+\frac{1}{2},j,k} + CB_m\left[\frac{1}{\kappa_y\Delta y}\sum_l a(l) H^{\phi z,n+\frac{1}{2}}_{i+\frac{1}{2},j+l+\frac{1}{2},k}\right.$$
$$\left. -\frac{1}{\kappa_z\Delta z}\sum_l a(l) H^{\phi y,n+\frac{1}{2}}_{i+\frac{1}{2},j,k+l+\frac{1}{2}}\right] + CB_m\left(\varphi^{\phi x,n+\frac{1}{2}}_{e_{xy},i+\frac{1}{2},j,k} - \varphi^{\phi x,n+\frac{1}{2}}_{e_{xz},i+\frac{1}{2},j,k}\right) \quad (23)$$

$$\varphi^{\phi x,n+\frac{1}{2}}_{e_{xy},i+\frac{1}{2},j,k} = P^y_j \varphi^{\phi x,n-\frac{1}{2}}_{e_{xy},i+\frac{1}{2},j,k} + Q^y_j \sum_l a(l)\frac{H^{\phi z,n+\frac{1}{2}}_{i+\frac{1}{2},j+l+\frac{1}{2},k}}{\Delta y} \quad (24)$$

$$\varphi^{\phi x,n+\frac{1}{2}}_{e_{xz},i+\frac{1}{2},j,k} = P^z_k \varphi^{\phi x,\,n-\frac{1}{2}}_{e_{xz},i+\frac{1}{2},j,k} + Q^z_k \sum_l a(l)\frac{H^{\phi y,n+\frac{1}{2}}_{i+\frac{1}{2},j,k+l+\frac{1}{2}}}{\Delta z} \quad (25)$$

where

$$P^y_j = \frac{2\varepsilon'_{y,j} - \alpha'_{y,j}\Delta t}{2\varepsilon'_{y,j} + \alpha'_{y,j}\Delta t} \quad (26)$$

$$Q^y_j = \frac{2\sigma'_{y,j}\Delta t}{2\varepsilon'_{y,j} + \alpha'_{y,j}\Delta t} \quad (27)$$

the CA_m, CB_m are the same with (5) and (6), and definitions for P_k^z and Q_k^z are similar with P_j^y and Q_j^y.

Observing (23)–(25), it is seen that the explicit time-marching schemes for the field and the auxiliary variables are obtained at the $(n+1)$ time step. And the schemes satisfied the stability condition for the S-MRTD scheme [2]. It is also obvious that the CFS-PML implementation requires no more than two auxiliary variables per field component, which is less than that reported by previous implementation of this method [25]. Therefore, the CFS-PML method is more straightforward and memory saving. Moreover, we use perfectly electric conductor (PEC) walls to terminate the PML regions.

Equations for E_y and E_z are as follow:

$$E_{i,j+\frac{1}{2},k}^{\phi y,n+1}=CA_m E_{i,j+\frac{1}{2},k}^{\phi y,n}+CB_m\left[\frac{1}{\kappa_z\Delta z}\sum_l a\left(l\right)H_{i,j+\frac{1}{2},k+l+\frac{1}{2}}^{\phi x,n+\frac{1}{2}}\right.$$
$$\left.-\frac{1}{\kappa_x\Delta x}\sum_l a\left(l\right)H_{i+\frac{1}{2},j+l+\frac{1}{2},k}^{\phi z,n+\frac{1}{2}}\right]+CB_m\left(\varphi_{e_{yz},i,j+\frac{1}{2},k}^{\phi y,n+\frac{1}{2}}-\varphi_{e_{yx},i,j+\frac{1}{2},k}^{\phi y,n+\frac{1}{2}}\right) \quad (28)$$

$$E_{i,j,k+\frac{1}{2}}^{\phi z,n+1}=CA_m E_{i,j,k+\frac{1}{2}}^{\phi z,n}+CB_m\left[\frac{1}{\kappa_x\Delta x}\sum_l a\left(l\right)H_{i+l+\frac{1}{2},j,k+\frac{1}{2}}^{\phi y,n+\frac{1}{2}}\right.$$
$$\left.-\frac{1}{\kappa_y\Delta y}\sum_l a(l)H_{i,j+l+\frac{1}{2},k+\frac{1}{2}}^{\phi x,n+\frac{1}{2}}\right]+CB_m\left(\varphi_{e_{zx},i,j,k+\frac{1}{2}}^{\phi z,n+\frac{1}{2}}-\varphi_{e_{zy},i,j,k+\frac{1}{2}}^{\phi z,n+\frac{1}{2}}\right) \quad (29)$$

The other set of equations for updating **H** can be obtained by duality.

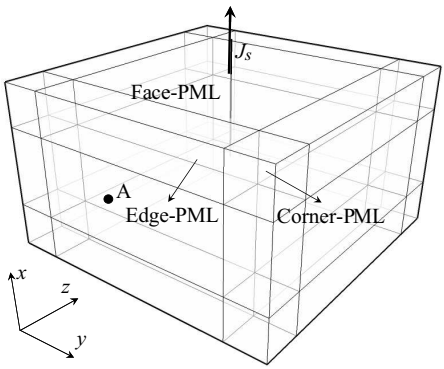

Figure 3. Computational model.

3.2. Result of the Reflection Error

To demonstrate CFS-PML termination of the S-MRTD lattice, a 3-D lattice of the dimension $Nx \times Ny \times Nz = 36 \times 36 \times 22$ was used, surrounding a computational domain of the dimension $20 \times 20 \times 6$ with a PML layer 8-cell thick. The media with constitutive parameters $\varepsilon_r = 7.0$ and $\sigma = 0.3$ is introduced into the computational domain. As shown in Fig. 3, the excitation was applied to the electric field component E_x at the center of the computation domain as follows:

$$E_{i,j}^{\phi z,n+1} = E_{i,j}^{\phi z,n} - \frac{(n\Delta t - 3t_0)}{t_0} \exp\left(-\frac{(n\Delta t - 3t_0)^2}{t_0^2}\right) \tag{30}$$

where $t_0 = 2.0\,\text{ns}$. The space is discretized with a mesh with $\Delta x = \Delta y = \Delta z = 0.05\,\text{m}$, and the time step is $\Delta t = 55.556\,\text{ps}$. Within the PML layer, the constitutive parameters σ_i and κ_i are scaled using a pth order polynomial scaling [31],

$$\sigma(\rho) = \sigma_{\max}\left(\frac{\rho}{d}\right)^p \tag{31}$$

$$\kappa(\rho) = 1 + (\kappa_{\max} - 1)\left(\frac{\rho}{d}\right)^p \tag{32}$$

where ρ denotes the distance from the interface of the computational domain and the PML into the PML layer, d is the depth of the PML, and p is the order of the polynomial. A choice for $\sigma_{\max}$ can be expressed as

$$\sigma_{opt} = \frac{(m+1)}{150\pi\sqrt{\varepsilon_r}\Delta} \tag{33}$$

where Δ is the grid spacing along the normal axis and there is no difference between x-, y-, and z-direction in all computations in this article. Another PML parameter α is not scaled, and is constant through the PML. In this article, the reflection error was computed at the sampling point A that corresponding to E_x a cell from the PML interface, where electromagnetic wave is incident normally. In order to isolate the error due to the PML from grid dispersion error, a reference problem was also simulated: the same mesh is extended 100 cells out in all dimensions, leading to a $236 \times 236 \times 222$ cell lattice. The error relative to reference solution was then computed as

$$error_{\text{dB}} = 20\log_{10}\frac{\left|E_x(t) - E_{x_{ref}}(t)\right|}{\max\left|E_{x_{ref}}(t)\right|} \tag{34}$$

where $E_x(t)$ represents the time-dependent discrete field computed within the working volume of the $36\times36\times22$ lattice, $E_{x_{ref}}(t)$ represents the same discrete field computed by the reference problem.

It is instructive to observe the maximum reflection error experienced by the CFS-PML method with ADE as a function of the constitutive parameters $\kappa_{\max}$, $\sigma_{\max}$ and α. Fig. 4 shows the contour plots of the maximum relative error over 900 time steps at point A versus $\kappa_{\max}$ and $\sigma_{\max}$ with $\alpha = 0.001$. It can be demonstrated that as low as -120 dB maximum error is achieved.

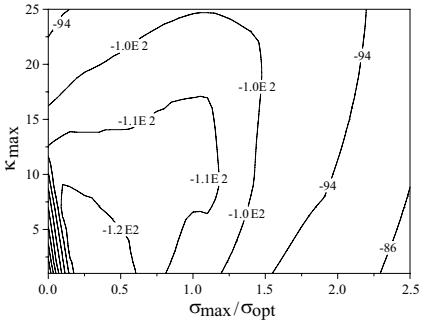

Figure 4. Contour plots of the maximum relative error for the first 900 time steps (CFS-PML).

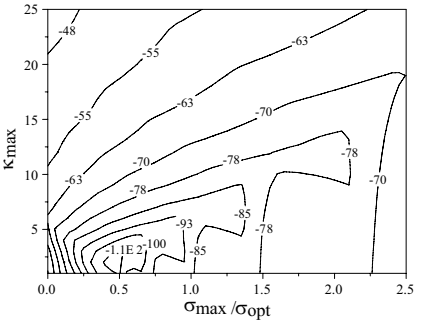

Figure 5. Contour plots of the maximum relative error for the first 900 time steps (APML).

Figure 5 does the same with the same $\kappa_{\max}$ and $\sigma_{\max}$ as Fig. 2 but for the APML. It can be seen that the maximum error is on the order of -63 dB. Compared with the APML, a dramatic improvement of nearly 60 dB is obtained with the CFS-CPML. Moreover, the optimal error is realized over a much broader range of $\kappa_{\max}$ and $\sigma_{\max}$, making these values easier to predict.

3.3. Implementation of the Parallel CFS-PML

For the sake of simplicity, the parallel implementation for the CFS-PML is also based on the one-dimension domain decomposition method. The material characteristics of each cell in the entire computation domain and the corresponding coefficients associated with the MRTD updating equations are stored in three-dimensional arrays. From Eqs. (23)–(25), it can be seen that the governing equations are the same for the fields inside the CFS-PML and the inner sub-domains. Thus the most important thing for CFS-PML is to assign appropriate material characteristic to each cell.

To implement this in parallel code, we first define a temporary three-dimensional array for the entire computational space on each processor. After assigning appropriate material characteristic to each cell, the required material characteristic array of each processor can be

extracted form the temporary one according to the processor position. Such processing method is straightforward and easy to implement, moreover, it is not necessary to decide which processor a specific cell belongs to, thus saving CPU time.

4. APPLICATION OF THE PARALLEL MRTD ALGORITHMS

EMP propagation in tunnel is a significant subject to study, the interest stems from two application areas: electromagnetic protection against the EMP weapons, which are mainly of interest for the military applications and the ultra-wideband (UWB) communication in tunnel which driven by the commercial application. When predominating the characteristic of the field cross-section distribution of the EMP propagation in tunnel, we could install the sensitive electromagnetic devices or the shielding equipments such as wave-guide widows, metallic doors and filters at the place where the filed distribution is weak, or change the distributed direction of some components to weaken the coupling energy. For the wireless communication, we could install the antennae at the place where the field distribution is strong to get high coupling energy.

4.1. Model of the Tunnel

The compendious model of the vaulted tunnel is illustrated in Figs. 6 and 7. The dimensions of the tunnel cross-section are shown in

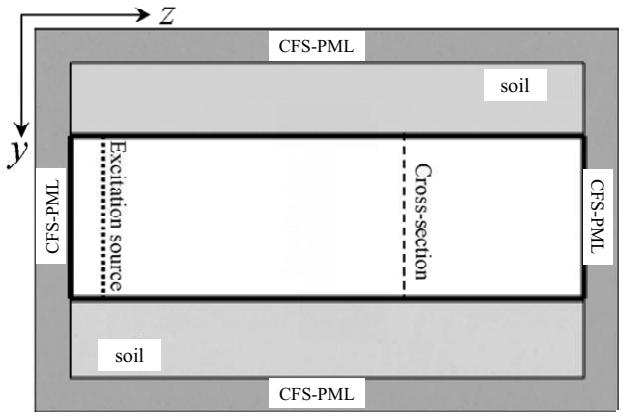

Figure 6. The computational model of the tunnel.

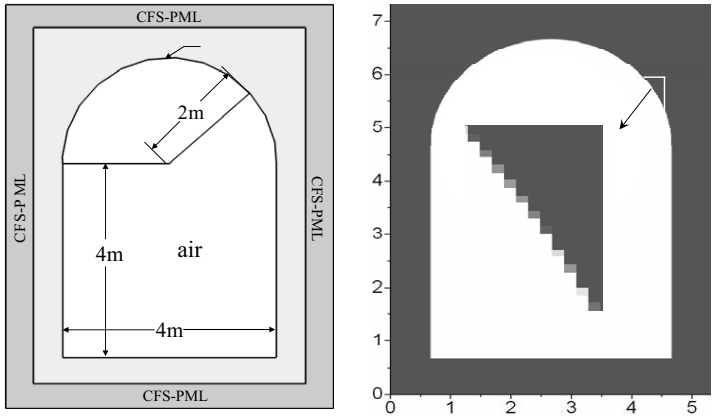

Figure 7. Profile of the computational model. (a) The cross-section of the tunnel. (b) The conformed vault of the tunnel.

Fig. 7(a). The source is placed near the CFS-PML. For the purposes of this study, constitutive parameters for soil were assumed, giving $\sigma_s = 0.004$, $\varepsilon_{rsoil} = 9.0$. The constitutive parameters for the wall and arris of the straight part can be defined as

$$\text{wall:}\quad \varepsilon_{eq} = 9.0,\ \ \sigma_{eq} = \frac{\sigma_s}{2},\quad \text{arris:}\quad \varepsilon_{eq} = \frac{3\varepsilon_0\varepsilon_r + \varepsilon_0}{4},\ \ \sigma_{eq} = \frac{3\sigma_s}{4}$$

Following the procedure of [32], the conformal technique in [32] can be also used here. Then the constitutive parameters for the wall and arris of the crooked part can be defined via the conformal technique. The conformed vault of the tunnel is shown as Fig. 7(b).

4.2. Setting the Excitation Source

In the waveguide system [33], the excitation source is usually introduced robustly according to propagation model such as TE_{10}, TM_{11}, etc.. Though in this case we can't get the analytical model of the wave propagation, the way that the excitation sources induced in the waveguide system can still be employed here, which can be showed as follows

$$E_{\tan}^{n+1}(i,j,k_s) = E_{\tan}^{n}(i,j,k_s) + f(i,j,k_s)g(t) \tag{35}$$

where the subscript 'tan' denotes the E-field distributed in a transverse cross section at $z = k_s\Delta z$ of the tunnel structure in Fig. 6, $f(i,\ j,\ k_s)$ is the function of the field distribution and $g(t)$ refer to the time function

determine the bandwidth of the sources. Here we set $f(i, j, k_s)$ as the model of TM_{11} propagation in waveguide approximately, though the model doesn't satisfy the boundary condition of the tunnel, we could believe that after the wave propagating a certain length, the model will be in a steady state which approach TM_{11} propagation model of the tunnel itself.

TM_{11} propagation model is defined as

$$\left.\begin{aligned} E_x &= -\frac{j\beta_{11}}{k_c^2}\frac{\pi}{a}A\cos\left(\frac{\pi}{a}x\right)\sin\left(\frac{\pi}{b}y\right)e^{-j\beta_{11}z}, \\ E_y &= -\frac{j\beta_{11}}{k_c^2}\frac{\pi}{b}A\sin\left(\frac{\pi}{a}x\right)\cos\left(\frac{\pi}{b}y\right)e^{-j\beta_{11}z} \\ E_z &= A\sin\left(\frac{\pi}{a}x\right)\sin\left(\frac{\pi}{b}y\right)e^{-j\beta_{11}z} \\ H_x &= \frac{j\omega\varepsilon}{k_c^2}\frac{\pi}{b}A\sin\left(\frac{\pi}{a}x\right)\cos\left(\frac{\pi}{b}y\right)e^{-j\beta_{11}z}, \\ H_y &= -\frac{j\omega\varepsilon}{k_c^2}\frac{\pi}{a}A\cos\left(\frac{\pi}{a}x\right)\sin\left(\frac{\pi}{b}y\right)e^{-j\beta_{11}z} \\ H_z &= 0 \end{aligned}\right\} \tag{36}$$

$g(t)$ in (12) set to be a differential Gaussian electric pulse that $g(t) = E_0(t - t_0)\exp(4\pi(t - t_0)^2/\tau^2)$ with $\tau = 3.0\,\text{ns}$, $E_0 = 1000\,\text{V/m}$ and $t_0 = \tau$.

4.3. Feasibility and Application of the Parallel MRTD Algorithms

To check whether the parallel implementation is feasible or not, comparison between serial MRTD and parallel MRTD is executed to analyze the proposed problem. Here we define that the tunnel is 45 m long, the space is discretized with an MRTD lattice with $\Delta x = \Delta y = \Delta z = 0.03\,\text{m}$, ten-cell-thick PML layers terminate the grid. This results in a $260 \times 173 \times 1720$ cell lattice, and time step is $\Delta t = 33.333\,\text{ps}$. $f(i, j, k_s)$ is located at the x-y plane with $z = 0.3\,\text{m}$, the sampling point is located at the center of x-y plane with $z = 43\,\text{m}$ The simulation is performed for 10000 time steps. The computational domain is divided in the z-direction because of its high efficiency of data exchange and the property of the computational model.

The computational requirement is enabled to be executed on a single PC. Here the hardware platform of the PC is as follows: Intel(R) Core(TM) i7 2.93 GHz CPU, 7.93GB Memory; and the software platform: Microsoft Windows XP Professional, Fortran 90 Complier,

MPICH2-1.0.6-WIN32-IA32 Software. We use the serial MRTD and parallel MRTD (4 PC nodes) to compute the case, and then compare the electric field E_y at the reference point.

As shown in Fig. 8, we can conclude that parallel MRTD gives the same result as serial MRTD dose. But the serial MRTD will be helpless when more grids are involved in simulating the tunnel, and then only parallel MRTD can work.

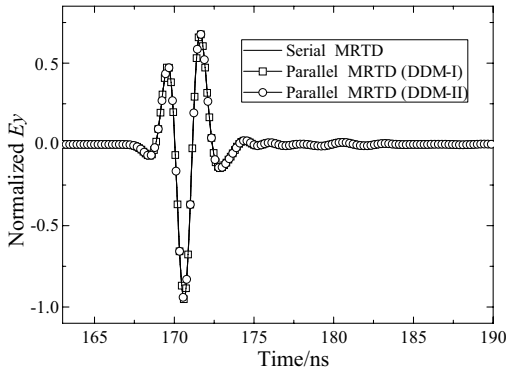

Figure 8. Comparison between serial MRTD and parallel MRTD.

In order to identify which parallel approach is more efficient, a comparison work is carried out here. As shown in Table 1, where T_1 is the execution time on one processor (serial MRTD), and T_n is the execution time on n processors, we can see that the execution time is not reduced by a factor n, this is because some fields around the processor boundary will require a small amount of information from the neighboring processors, those required data values from the MRTD gird on neighboring processors are thus exchanged, and this communication introduces an overhead into the parallel MRTD code that is not present in the serial form. Moreover, it is obvious that the DDM-I is a little more efficient than DDM-II, and this is because that the total number of the exchanged data is the same in both approaches, but the $E_{x,y}$ fields shown in Section 3, part II are updated twice in DDM-II, which results in more execution time.

Next, using the parallel MRTD (DDM-I), we define that the tunnel is 200 m long, the space and time step, $f(i, j, k_s)$ are the same as before. This results in a $260 \times 173 \times 7020$ cell lattice, and the simulation is performed for 20000 time steps. A sampling cross-section is located at the x-y plane with $z = 150$ m. As it's difficult to get the analytic result of the field cross-section distribution with different

Table 1. (a) Performance increase against the number of processors (DDM-I). (b) Performance increase against the number of processors (DDM-II).

(a)

Number of Processors	Execution Time/s	Speed up $S_p = T_1/T_n$	Efficiency $\eta = S_p/n$
1	556.4	1	100%
2	394.6	1.41	70.5%
3	268.8	2.07	69.0%
4	209.2	2.66	66.5%

(b)

Number of Processors	Execution Time/s	Speed up $S_p = T_1/T_n$	Efficiency $E = S_p/n$
1	556.4	1	100%
2	406.1	1.37	68.3%
3	278.2	2.00	66.6%
4	213.2	2.61	65.1%

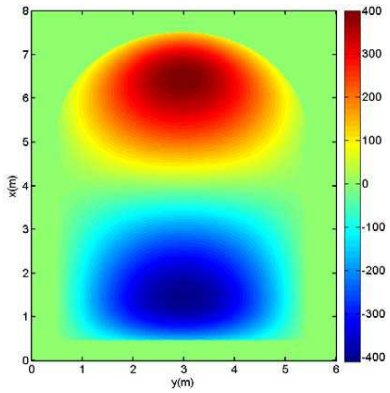

(a)

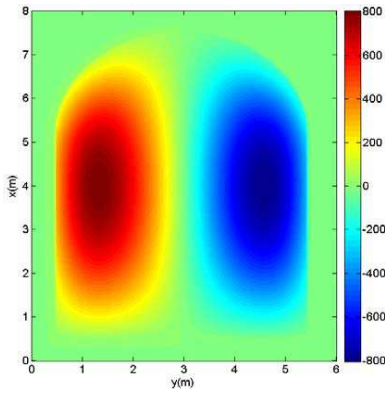

(b)

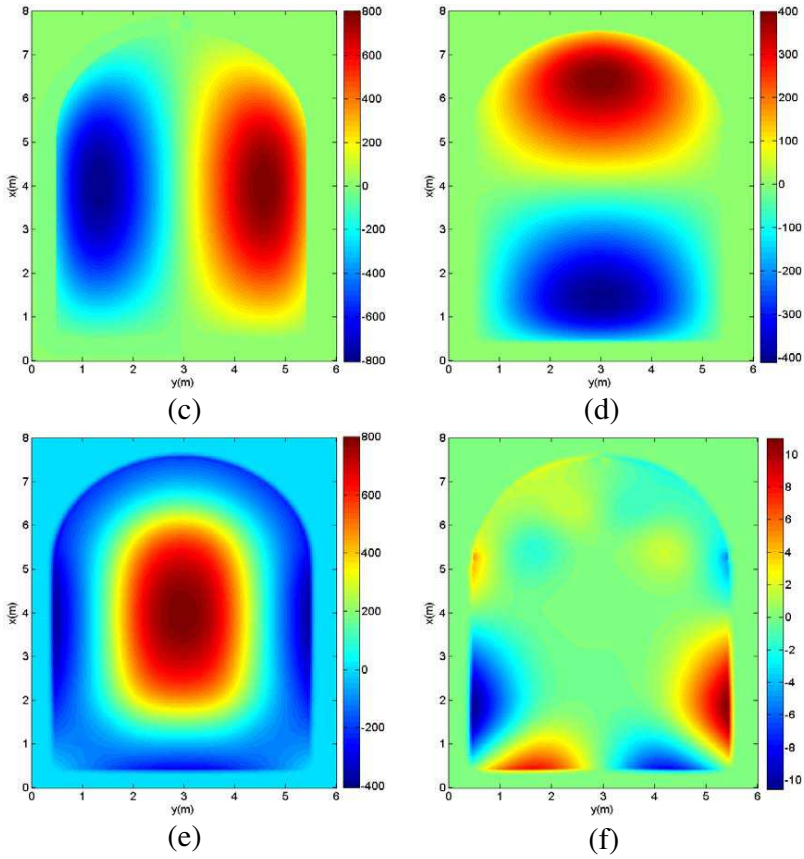

Figure 9. The cross-section distributions of the fields. (a) E_x (V/m). (b) H_x (A/m). (c) E_y (V/m). (d) H_y (A/m). (e) E_z (V/m). (f) H_z (A/m).

excitation propagation models, the result from numerical simulation is all-important for the engineering underground.

Figures 9(a)–9(f) denote the cross-section distributions of the fields of **E** and **H** in the tunnel. Observing the results, it is seen that the mainly characteristics of the fields' distributions are generally similar with that in the perfect waveguide. Though the field H_z is not zero, it is very small compared with the other five fields. And the distribution characteristics for E_x and H_y, E_y and H_x are similar, which can be validated from Eq. (36). Take E_x as example, E_x has two peaks along the x-direction, one of which is positive, the other one is negative. Moreover, the E_z, field basically distributes as the stationary wave along the x and y coordinates, and the energy of E_z field is mainly located in the middle area of the cross-section.

5. CONCLUSION

In this paper, we present two parallel MRTD approaches. Details about the implementations of the domain decomposition, message passing between the neighboring processors and CFS-PML with ADE are also provided. Numerical results show that both methods are feasible, and the DDM-I is more efficient than DDM-II. The proposed method of CFS-PML with ADE is more straightforward to implement compared with conventional APML. Numerical examples show that maximum errors on the order of $-120\,\mathrm{dB}$ were recorded for the CFS-PML, compared to $-110\,\mathrm{dB}$ for the APML. And a striking advantage of CFS-PML with ADE is that the optimal reflection error can be realized over a much broader range of $\kappa_{\max}$ and $\sigma_{\max}$, making these values easier to obtain. Moreover, the computational model of a vaulted tunnel is established, and the characteristics of the fields' cross-section distributions of the TM_{11} propagation model in the vaulted tunnel is obtained and analyzed.

ACKNOWLEDGMENT

The authors would like to acknowledge the reviewers for helpful remarks.

REFERENCES

1. Krumpholz, M. and L. P. B. Katehi, "New prospects for time domain analysis," *IEEE Microwave Guid Wave Lett.*, Vol. 5, No. 11, 382–384, Dec. 1995.
2. Krumpholz, M. and L. P. B. Katehi, "MRTD: New time-domain schemes based on multiresolution analysis," *IEEE Trans. on Microwave Theory and Tech.*, Vol. 44, No. 4, 555–561, Apr. 1996.
3. Sirenko, K., V. Pazynin, Y. K. Sirenko, and H. Bağci, "An FFT-accelerated FDTD scheme with exact absorbing conditions for characterizing axially symmetric resonant structures," *Progress In Electromagnetics Research*, Vol. 111, 331–364, 2011.
4. Lee, K. H., I. Ahmed, R. S. M. Goh, E. H. Khoo, E. P. Li, and T. G. G. Hung, "Implementation of the FDTD method based on lorentz-drude dispersive model on GPU for plasmonics applications," *Progress In Electromagnetics Research*, Vol. 116, 441–456, 2011.
5. Izadi, M., M. Z. A. Ab Kadir, and C. Gomes, "Evaluation of electromagnetic fields associated with inclined lightning

channel using second order FDTD-hybrid methods," *Progress In Electromagnetics Research*, Vol. 117, 209–236, 2011.

6. Vaccari, A., A. Cala' Lesina, L. Cristoforetti, and R. Pontalti, "Parallel implementation of a 3D subgridding FDTD algorithm for large simulations," *Progress In Electromagnetics Research*, Vol. 120, 263–292, 2011.
7. Kong, Y.-D. and Q.-X. Chu, "Reduction of numerical dispersion of the six-stages split-step unconditionally-stable FDTD method with controlling parameters," *Progress In Electromagnetics Research*, Vol. 122, 175–196, 2012.
8. Kong, L.-Y., J. Wang, and W.-Y. Yin, "A novel dielectric conformal FDTD method for computing SAR distribution of the human body in a metallic cabin illuminated by an intentional electromagnetic pulse (IEMP)," *Progress In Electromagnetics Research*, Vol. 126, 355–373, 2012.
9. Mao, Y., B. Chen, H.-Q. Liu, J.-L. Xia, and J.-Z. Tang, "A hybrid implicit-explicit spectral FDTD scheme for oblique incidence problems on periodic structures," *Progress In Electromagnetics Research*, Vol. 128, 153–170, 2012.
10. Wang, J.-B., B.-H. Zhou, L.-H. Shi, C. Gao, and B. Chen, "A novel 3-D weakly conditionally stable FDTD algorithm," *Progress In Electromagnetics Research*, Vol. 130, 525–540, 2012.
11. Xiong, R., B. Chen, Y. Mao, B. Li, and Q.-F. Jing, "A simple local approximation FDTD model of short apertures with a finite thickness," *Progress In Electromagnetics Research*, Vol. 131, 135–152, 2012.
12. Xiong, R., B. Chen, J.-J. Han, Y.-Y. Qiu, W. Yang, and Q. Ning, "Transient resistance analysis of large grounding systems using the FDTD method," *Progress In Electromagnetics Research*, Vol. 132, 159–175, 2012.
13. Gradoni, G., V. Mariani Primiani, and F. Moglie, "Reverberation chamber as a multivariate process: FDTD evaluation of correlation matrix and independent positions," *Progress In Electromagnetics Research*, Vol. 133, 217–234, 2013.
14. Kong, Y.-D., Q.-X. Chu, and R.-L. Li, "High-order unconditionally-stable four-step adi-FDTD methods and numerical analysis," *Progress In Electromagnetics Research*, Vol. 135, 713–734, 2013.
15. Chun, K., H. Kim, H. Kim, and Y. Chung, "PLRC and ADE implementations of drude-critical point dispersive model for the FDTD method," *Progress In Electromagnetics Research*, Vol. 135, 373–390, 2013.

16. Stefanski, T. P., "Implementation of FDTD-compatible Green's function on heterogeneous CPU-GPU parallel processing system," *Progress In Electromagnetics Research*, Vol. 135, 297–316, 2013.
17. Wang, W., P.-G. Liu, and Y.-J. Qin, "An unconditional stable 1D-FDTD method for modeling transmission lines based on precise split-step scheme," *Progress In Electromagnetics Research*, Vol. 135, 245–260, 2013.
18. Donelli, M., I. Craddock, D. Gibbins, and M. Sarafianou, "A three dimensional time domain microwave imaging method for breast cancer detection based on an evolutionary algorithm," *Progress In Electromagnetic Research M*, Vol. 18, 179–195, 2011.
19. Johnson, J., T. Takenaka, K. A. Hong Ping, S. Honda, and T. Tanaka, "Advances in the 3-D forward-backward time stepping (FBTS) inverse scattering technique for breast cancer detection," *IEEE Trans. on Biomed. Eng.*, Vol. 56, No. 9, 2232–2243, 2009.
20. Moriyama, T., T. Takenaka, and Z. Meng, "Forward-backward time stepping method combined with genetic algorithm applied to breast cancer detection," *Microwave and Optical Technology Letters*, Vol. 53, No. 2, 438–442, 2009.
21. Cheong, Y. W., Y. M. Lee, K. H. Ra, J. G. Kang, and C. C. Shin, "Wavelet-Galerkin scheme of time-dependent inhomogeneous electromagnetic problems," *IEEE Microwave Guid Wave Lett.*, Vol. 9, No. 8, 297–299, Aug. 1999.
22. Fujii, M. and W. J. R. Hoefer, "Dispersion of time domain wavelet Galerkin method based on Daubechies' compactly supported scaling functions with three and four vanishing Moments," *IEEE Microwave Guid Wave Lett.*, Vol. 10, No. 4 125–127, Apr. 2000.
23. Guiffaut, C., and K. Mahdjoubi, "A parallel FDTD algorithm using the MPI library," *IEEE Antennas and Propagation Magazine*, Vol. 43, 94–103, Apr. 2001.
24. Wang L. and C. Liang, "A new implementation of CFS-PML for ADI-FDTD method," *Microwave and Optical Technology Letters*, Vol. 48, No. 10, 1924–1928, Oct. 2006.
25. Cao, Q. and Y. Chen, "Application of an anisotropic perfectly matched layer absorber for open boundary truncation in the multiresolution time domain scheme," *IEEE Trans. on Antennas and Propagat.*, Vol. 51, No. 2, 350–357, Feb. 2003.
26. Daubechies, I., *Ten Lectures on Wavelets*, SIAM, Philadelphia, PA, 1992.
27. Sweldens, W. and R. Piessens, "Wavelet sampling techniques," *Proc. Statistical Computing Section*, 20–29, 1993.

28. Liu, Y., Y.-W. Chen, P. Zhang, and X. Xu, "Implementation and application of the spherical MRTD algorithm," *Progress In Electromagnetics Research*, Vol. 139, 577–597, 2013.
29. Chew, W. C. and W. H. Weedon, "A 3D perfectly matched medium from modified Maxwell's equations with stretched coordinates," *Microwave and Optical Technology Letters*, Vol. 7, No. 7, 599–604, Sep. 1994.
30. Kuzuoglu, M. and R. Mittra, "Frequency dependence of the constitutive parameters of causal perfectly matched anisotropic absorbers," *IEEE Microwave Guid Wave Lett.*, Vol. 6, 447–449, Dec. 1996.
31. Gedney, S. D., G. Liu, J. A. Roden, and A. Zhu, "Perfectly matched layer media with CFS for an unconditionally stable ADI-FDTD method," *IEEE Trans. on Antennas and Propagat.*, Vol. 49, 1554–1559, Nov. 2001.
32. Yu, W. and M. Raj, "A conformal finite difference time domain technique for modeling curved dielectric surfaces," *IEEE Microwave and Wireless Components Letters*, Vol. 11, No. 1, 25–27, Jan. 2001.
33. Taflove, A., *Computational Electrodynamics: the Finite-difference Time-domain Method*, Artech House, Norwood, MA, 1995.